Homogenization for composite material properties using smoothed finite element method

Eric Li[1*], Zhongpu Zhang[1], CC Chang[1], GR Liu[2], Q Li[1]

[1]*School of Aerospace, Mechanical and Mechatronic Engineering, The University of Sydney, Sydney, NSW 2006, Australia*

[2]*School of Aerospace Systems, University of Cincinnati, Cincinnati, OH 45221-0070, USA*

Abstract

Numerical homogenization is an efficient way to determine effective material properties of composite materials. Conventionally, the finite element technique has been widely used in implementing the homogenization. However, the standard finite element method (FEM) leads to an overly-stiff model which gives poor accuracy especially using triangular elements in 2D or tetrahedral elements in 3D with coarse mesh. In this paper, the smoothed finite element methods (S-FEMs) are developed to analyse the effective mechanical properties of composite materials. Various examples, including modulus with multiphase composites and permeability of tissue scaffold, have demonstrated that smoothed finite element method is able to provide more accurate results using the same set of mesh compared with the standard finite element method. In addition, the computation efficiency of smoothed finite element method is also much better than the FEM counterpart.

Keywords: smoothed finite element methods, homogenization, composite material, Tissue Scaffold

[1*]Corresponding author.

Email address: ericsg2012@gmail.com

1. Introduction

Attributable to its more versatile and tuneable material properties, a range of composites has been widely used in aerospace, marine, vehicle and biomedical industry as shown in Fig. 1. Their different microstructures with two or more constituents allow achieving desirable properties such as multi-functionality and lightweight. To control the material properties, the spatial layout of the microstructure and/or the compositions of the constituent phases are extremely important [1]. However, it is always cumbersome to tweak a most appropriate microstructure and characterize its effective properties effectively [2].

Substantial research has been done in the evaluation of effective (or namely bulk) elastic properties of composite materials. An early attempt for the design of composite material is perhaps the bounds of material property. Using variational principles, Hashin and Shtrikman developed theoretical bounds for the bulk (K) and shear (G) moduli of two-phases, well-ordered materials [3]. Following this, some improvements of material bounds have been extended to multi-phase, multi-dimensional composites for various physical properties [4-5]. Although property bounds give the constraint of effective properties and provide some clue in choosing different phases for composite design, these all require additional information regarding the geometric layout of the microstructure [6].

Numerical homogenization is an effective way to quantify the material properties based on an asymptotic expansion of the governing equations [7-11]. In the numerical homogenization, it is assumed that the representative volume element (RVE) or unit cell is locally repeated with very small microstructure compared with the overall 'macroscopic' dimensions of the structure of interest, in which the different materials are bonded in the RVE. The homogenization method is based on a rigorous mathematical theory [12], and it can provide us with a reasonable solution for some material design problems, where experimental techniques may be very costly or unavailable, apart from the determination of theoretical bounds for an estimation purpose [13].

Currently, FEM is the most popular method in numerical homogenization for composite material properties [14-18]. However, FEM has some inherent drawbacks which limit the development of numerical homogenization. The first issue is its “overly stiff” phenomenon of a fully compatible FEM model [19, 20]; the second concerns with the mesh distortion related problems such as the significant accuracy loss when the element mesh is heavily distorted; the third is the poor accuracy in the stress solution using triangular in 2D or tetrahedral elements in 3D.

Due to this reason, Liu and his co-authors have established a weakened weak (W2) formulation using the generalized gradient smoothing technique to unify all the developed numerical methods [21]. The W2 formulation seeks solutions in the so-called G space, which includes both continuous and discontinuous functions. Hence, it works for both compatible and incompatible displacements in the framework of the finite element and meshfree methods. Using the generalized strain smoothing technique, the Smoothed Point Interpolation Methods (S-PIMs) [22] have been developed, which offers a number of outstanding features. With the strain smoothing technique [23], the smoothed finite element methods (S-FEMs) have been proposed to overcome the shortcoming of FEM model [24-25]. The S-FEMs can be viewed as the simplest linear version of S-PIMs and has the advantages of simplicity and yet outstanding performance and important features.

Compared with overly-stiff FEM, S-FEMs provides a softened system model for high convergence and accuracy. According to smoothing algorithm, several different formulations, namely cell-based smoothed FEM (CS-FEM) [26-27], node-based smoothed FEM (NS-FEM) [28], and edged-based smoothed FEM (ES-FEM) [29-30], have been proposed respectively. These methods introduce the strain smoothing operations to the standard FEM procedures, and worked fairly effectively for a range of engineering problems such as solid mechanics [31], heat transfer [32-35] and acoustics [36-37]. The implementation of such smoothed finite element methods is quite straightforward without additional parameters involved. The study of S-FEMs has also clearly shown that the smoothing operation on strains allows to manipulate the assumed strain field in a proper fashion to ensure the stability (boundness), thus ensuring the (monotonic) convergence, and giving the S-FEMs some very good features.

Lured by the special properties of smoothed finite element methods, this study for the first time attempted to formulate homogenization problem for different composite materials. The objective to develop S-FEMs for homogenization is to improve the numerical accuracy, computational efficiency, as well as to study the applicability of S-FEMs. The above mentioned various smoothed finite element techniques are formulated here to characterize the effective properties for two or more materials. This paper is organized as follows: Section 2 briefs numerical homogenization using finite element methods. Section 3 presents the formulation of smoothed finite element methods in numerical homogenization. The 2D and 3D demonstrative examples are shown in Section 4 to verify the applicability of smoothed finite element method in numerical homogenization. The conclusions are drawn in Section 5.

2. Brief of numerical homogenization using FEM

2.1 Concept of Periodic Representative Volume Element (RVE)

In this study, we consider periodic composites which comprise repetitive identical unit cells in the microscopic level of material structure. For the sake of simplicity, only two-dimensional problem is illustrated here as shown Fig. 2. To characterize one piece of material sample, the computational cost for a full finite element (FE) model can be extremely high as discretization of the whole sample solid becomes enormous in order to represent detailed structure of the microscopic material constitutions. Such issue will be more serious and could become prohibitive in three-dimensional problems. Fortunately, the homogenization method provides an efficient way to predict the mechanical behaviour of macrostructure without modeling the entire macroscopic structure of multiphase composites [12].

In general, the selection of representative volume element (RVE) is crucial in the homogenization process in order to accurately predict the effective mechanical properties. The selective RVE must make sure repetitive unit identifiable in the domain carry all the geometric features necessary to fully define the medium [38]. Note that while the RVE is not uniquely defined in the homogenization; the effective mechanical properties from different unit cells should be ideally the same on the given scale. Additionally, when deciding the size of the RVE, the geometrical and material symmetries of the structure can be considered in order to simplify the implementation of numerical code [17].

2.2 Effective Elastic Moduli

For more effective discussion, we first brief on the standard formulation of FEM in numerical homogenization [14, 15], as some of these formulae will be used repetitively in later sections. In the homogenization, two levels of coordinate systems are used: one is the global coordinate system of macrostructure y_i and another is the local coordinate system of microstructure x_i. In the following analysis, linear elastic constitutive law is assumed. The relationship between the local coordinate system x_i for the RVE and global coordinate system of sample macrostructure y_i can be written as follows [14, 15]:

$$x_i = \frac{y_i}{\varepsilon} \tag{1}$$

where ε is the small scaling parameter between these two length scales.

Based on asymptotic expansion, it is reasonable to approximate $\mathbf{u}^{\varepsilon}$ in the following form with respect to parameter ε

$$\mathbf{u}^{\varepsilon}(y) = \mathbf{u}^{0}(x,y) + \varepsilon \mathbf{u}^{1}(x,y) + \varepsilon^{2}\mathbf{u}^{2}(x,y) + \ldots \tag{2}$$

where the function $\mathbf{u}_i^0, \mathbf{u}_i^1, \mathbf{u}_i^2 \ldots$ are *X*-periodic with respect to the local coordinate *x*.

The strain-displacement and stress-strain relationships can be accordingly expressed as follows

$$\boldsymbol{\varepsilon}(\mathbf{y}) = \frac{1}{2}\left(\frac{\partial \mathbf{u}_k^{\varepsilon}}{\partial y_l} + \frac{\partial \mathbf{u}_l^{\varepsilon}}{\partial y_k}\right) \tag{3}$$

$$\boldsymbol{\sigma}\left(\mathbf{u}^{\varepsilon}\right) = \mathbf{D}\boldsymbol{\varepsilon}\left(\mathbf{u}^{\varepsilon}\right) \tag{4}$$

where **D,** $\boldsymbol{\varepsilon}$, $\mathbf{u}^{\varepsilon}$ $\boldsymbol{\sigma}$ are the elasticity matrix for base material, strain, displacement and stress.

As $\mathbf{u}_1$ is the first order variation from the average displacement, this variation can be considered to be proportional to the average strain $\boldsymbol{\varepsilon}_0$ [14]:

$$\mathbf{u}_1 = -\boldsymbol{\xi}(\mathbf{x})\boldsymbol{\varepsilon}_0(\mathbf{y}) \tag{5}$$

where $\boldsymbol{\xi}$ is the characteristic displacement function of the microstructure. In other words, the characteristic displacement is scaled directly by the average train because it is the displacement for the unit strain of the macrostructure.

From Eqs. (3)-(5), the total potential energy is formulated as follows [14]:

$$\Gamma\Gamma\left(\mathbf{u}^{\varepsilon}\right) = \frac{1}{|X|}\int_D \left(\mathbf{L}_{dy}\mathbf{u}_0\right)^{\mathrm{T}} \int_X \left(\mathbf{I} - \mathbf{L}_{dx}\boldsymbol{\xi}\right)^{\mathrm{T}} \mathbf{D}\left(\mathbf{I} - \mathbf{L}_{dx}\boldsymbol{\xi}\right)\left(\mathbf{L}_{dy}\mathbf{u}_0\right) dX \left(\mathbf{L}_{dy}\mathbf{u}_0\right) dD - \int_{\Gamma_T} \mathbf{u}_0^t \mathbf{t}\, d\Gamma \tag{6}$$

where $|X|$ is the area (volume in 3D) of RVE, $\mathbf{I}$ is the identity, and $\mathbf{L}_d$ is a matrix of differential operator defined as:

$$\mathbf{L}_{dx} = \begin{bmatrix} \partial/\partial \mathbf{x}_1 & 0 \\ 0 & \partial/\partial \mathbf{x}_2 \\ \partial/\partial \mathbf{x}_2 & \partial/\partial \mathbf{x}_1 \end{bmatrix}, \qquad \mathbf{L}_{dy} = \begin{bmatrix} \partial/\partial \mathbf{y}_1 & 0 \\ 0 & \partial/\partial \mathbf{y}_2 \\ \partial/\partial \mathbf{y}_2 & \partial/\partial \mathbf{y}_1 \end{bmatrix} \tag{7}$$

Define

$$\mathbf{D}^H = \frac{1}{|X|}\int_X \left(\mathbf{I}-\mathbf{L}_{dx}\boldsymbol{\xi}\right)^{\mathrm{T}} \mathbf{D}\left(\mathbf{I}-\mathbf{L}_{dy}\boldsymbol{\xi}\right) dX \tag{8}$$

and substitute Eq. (8) into (6) leads to

$$\Gamma\Gamma\left(\mathbf{u}^{\varepsilon}\right) = \int_D \left(\mathbf{L}_{dy}\mathbf{u}_0\right)^{\mathrm{T}} \mathbf{D}^H \left(\mathbf{L}_{dy}\mathbf{u}_0\right) dD - \int_{\Gamma_T} \mathbf{u}_0^t \mathbf{t} d\Gamma \tag{9}$$

The homogenized elasticity matrix $\mathbf{D}^H$ in Eq. (8) is obtained [14] through discretization of unit cell using finite element technique. In the numerical implementations, the FEM divides the domain Ω into a number of elements, and the following trial functions are used:

$$\boldsymbol{\xi}\left(\mathbf{x},\mathbf{d}\right) = \mathbf{N}_i\left(\mathbf{x}\right)\mathbf{d}_i \tag{10}$$

$$\mathbf{L}_{dx}\boldsymbol{\xi} = \mathbf{B}_i\mathbf{d}_i \tag{11}$$

where $\mathbf{d}_i$ is the vector of nodal displacements, and $\mathbf{N}_i\left(\mathbf{x}\right)$ is a matrix of shape function in the microstructure. The strain matrix $\mathbf{B}_i$ is defined as follows:

$$\mathbf{B}_i = \begin{bmatrix} \partial\mathbf{N}_i/\partial\mathbf{x}_1 & 0 \\ 0 & \partial\mathbf{N}_i/\partial\mathbf{x}_2 \\ \partial\mathbf{N}_i/\partial\mathbf{x}_1 & \partial\mathbf{N}_i/\partial\mathbf{x}_2 \end{bmatrix} \qquad \text{2D} \tag{12}$$

$$\mathbf{B}_i = \begin{bmatrix} \partial\mathbf{N}_i/\partial\mathbf{x}_1 & 0 & 0 \\ 0 & \partial\mathbf{N}_i/\partial\mathbf{x}_2 & 0 \\ 0 & 0 & \partial\mathbf{N}_i/\partial\mathbf{x}_3 \\ \partial\mathbf{N}_i/\partial\mathbf{x}_1 & \partial\mathbf{N}_i/\partial\mathbf{x}_2 & 0 \\ 0 & \partial\mathbf{N}_i/\partial\mathbf{x}_2 & \partial\mathbf{N}_i/\partial\mathbf{x}_3 \\ \partial\mathbf{N}_i/\partial\mathbf{x}_1 & 0 & \partial\mathbf{N}_i/\partial\mathbf{x}_3 \end{bmatrix} \qquad \text{3D} \tag{13}$$

Substitute Eq. (10) into Eq. (8), the effective mechanical properties can be written as follows:

$$\mathbf{D}^H = \frac{1}{|X|}\int_X \left(\mathbf{I}-\mathbf{B}_i\mathbf{d}_i\right)^{\mathrm{T}} \mathbf{D}\left(\mathbf{I}-\mathbf{B}_i\mathbf{d}_i\right) dX \tag{14}$$

In order to obtain an equilibrium state, one can set variational to zero,

$$\delta\mathbf{d}_i\left(\int_X \mathbf{B}_i\mathbf{D}dX - \int_X \mathbf{B}_i^T\mathbf{D}\mathbf{B}_i dX\mathbf{d}_i\right) = 0 \tag{15}$$

By substituting the approximations $\mathbf{d}_i$ into Equation (14) and invoking the arbitrariness of virtual nodal displacements, we have the standard discretized algebraic system equation:

$$\mathbf{K}\mathbf{d}^n = \mathbf{F}^n \tag{16}$$

where $\mathbf{K}$ is an analogized element stiffness matrix, and $\mathbf{F}^n$ is the nodal force vector which is equivalent to the initially applied strain field.

$$\mathbf{K} = \int_X \mathbf{B}_i^T \mathbf{D} \mathbf{B}_i dX_e \tag{17}$$

$$\mathbf{F}^n = \int_X \mathbf{B}_i \mathbf{D} dX_e \tag{18}$$

For a 2D elastic problem, n=1, 2, 3, for 3D elastic problem, n=1… 6. For a 2D heat conduction or fluidic permeability problem, n=1, 2, for 3D heat conduction or fluidic permeability problem, n=1, 2, 3. The boundary conditions for each case are listed in Tables 1 and 2. The detailed formulation of numerical homogenization method is available in many resources [14, 15, 17, 18]. Although the above process is derived from elasticity problem, the effective fluidic permeability can be calculated in the same way.

3. Implementation of S-FEMs in numerical homogenization

In the formulation of S-FEMs homogenization, the critical step is that the smoothed strain, instead of compatible strain, is used. The pre-process of mesh and implementation of boundary conditions are exactly the same as the standard FEM based homogenization. Hence, the computation of a smoothed strain is crucial to formulate S-FEMs based homogenization. In this section, several different strain smoothness algorithms are presented for homogenization.

3.1 Edge-based smoothed finite element method (ES-FEM)

In the formulation of ES-FEM based homogenization, the first step is to construct the smoothing domain. The local smoothing domains are constructed with respect to the edge of triangular elements such that $\Omega = \bigcup_{k=1}^{N_s} \Omega_k^s$ and $\Omega_i^s \cap \Omega_j^s = \varnothing$, $\forall i \neq j$, in which N_s is the number of smoothing domains and equals to the number of elemental edges in the scheme of ES-FEM. For the triangular elements in 2D or tetrahedral elements in 3D, the smoothing domain associated with edge *k* is created by connecting two endpoints of the edge to two centroids of the two adjacent elements as shown in Fig. 3(a). Extending the smoothing domain Ω_k^s in 3D problems, the sub-domain of the smoothing domain Ω_k^s for edge k located in the particular cell *j* can be obtained by connecting two end nodes of the edge to the centroids of the surface triangles and the centroid of cell *j*. The sub-smoothing-domain for edge *k* is one sixth region of this tetrahedral element.

With the edge-based smoothing technique, the smoothed strains can be computed using the compatible strains $\boldsymbol{\varepsilon} = \mathbf{L}\mathbf{u}$ from the following smoothing operation [39]:

$$\bar{\boldsymbol{\varepsilon}}_k = \frac{1}{A_k^s} \int_{\Gamma_k^s} \boldsymbol{\varepsilon}_k d\Gamma = \frac{1}{A_k^s} \int_{\Gamma_k^s} \mathbf{L}\mathbf{u} d\Gamma \tag{19}$$

where Γ_k^s is the boundary surface of the smoothing domain Ω_k^s, $A_k = \int_{\Omega_k^s} \mathrm{d}\Omega$ is the area of the smoothing domain for edge *k*, and **u** is the displacement vector expressed in the following approximate form:

$$\mathbf{u} = \sum_{i=1}^{N} \mathbf{N}_i (\mathbf{x}) \mathbf{d}_i = \mathbf{N}_s \mathbf{d} \tag{20}$$

where *N* is the number of field nodes per element and equals to 3 for the three-node triangular elements used in this work, $\mathbf{d}_i = \{ d_{xi} \quad d_{yi} \}^{\mathrm{T}}$ is the nodal displacement vector, **d** is the vector with all the N nodal displacements in the element, and $\mathbf{N}_i$ is a matrix of shape functions.

Substituting Eq. (20) into (19) and applying the divergence theorem, the smoothed strains for the smoothing domain Ω_k^s can then be obtained as follows

$$\bar{\boldsymbol{\varepsilon}}\left(\mathbf{x}_k\right)=\sum_{i=1}^{M_k}\bar{\mathbf{B}}_i^{\text{ES-2D}}\left(\mathbf{x}_k\right)\mathbf{d}_i \tag{21}$$

where M_k is the total number of nodes containing the same edge *i*. For the inner edge, M_k is equal to 4, and M_k becomes 3 for boundary edge.

The smoothed strain matrix can be calculated numerically in the following way:

$$\bar{\mathbf{B}}^{\text{ES-2D}}=\frac{1}{A^{(k)}}\sum_{j=1}^{N_e^{(k)}}\frac{1}{3}A_e^{(j)}\mathbf{B}_j^{\text{2D}} \tag{22}$$

where $N_e^{(k)}$ is the number of elements around the edge *k*. For the boundary edge, no smoothing effect exists in the edge, hence $N_e^{(k)}=1$ for boundary edges. For all inner edges, there are only two elements sharing one edge, so $N_e^{(k)}=2$.

The smoothed strain in 2D ES-FEM can be very straightforward to extend to 3D tetrahedral elements:

$$\bar{\mathbf{B}}^{\text{ES-3D}}=\frac{1}{V^{(k)}}\sum_{j=1}^{N_e^{(k)}}\frac{1}{6}V_e^{(j)}\mathbf{B}_j^{\text{3D}} \tag{23}$$

where V_e and $\mathbf{B}_j$ are the volume and the compatible strain gradient matrix of the *j*th tetrahedral element around node *k*, respectively. $V^{(k)}$ is calculated by the following equation:

$$V^{(k)}=\sum_{j=1}^{N_e^{(k)}}\frac{1}{6}V_e^{(j)} \tag{24}$$

Based on the formulations of smoothed strain expressed in Eqs. (22) and (23), the smoothed stiffness and force matrix can be written in the following forms, respectively:

$$\overline{\mathbf{k}}_{\mathrm{ES}} = \sum_{k\in N_e} \int_{\Omega^{(k)}} \left(\mathbf{B}_{\mathrm{ES}}\right)^{\mathrm{T}} \mathbf{D}\mathbf{B}_{\mathrm{ES}} d\Omega \tag{25}$$

$$\overline{\mathbf{F}}_{\mathrm{ES}} = \sum_{k\in N_e} \int_{\Omega^{(k)}} \left(\mathbf{B}_{\mathrm{ES}}\right)^{\mathrm{T}} \mathbf{D} d\Omega \tag{26}$$

For the multi-material formulation in ES-FEM, the process is similar to single material except the interface of different materials. As the material property is discontinuous along the interface, the associated smoothing domain will be separated into two regions as shown in Fig. 3(b), which is the same as it does along domain boundaries.

3.2 Node-based smoothed finite element method

Similar to ES-FEM, the smoothing domain is first constructed in the scheme of NS-FEM. For 2D problems with single material as shown in Fig. 3(a), the smoothing domain Ω_k^s for node *k* is constructed by connecting sequentially the mid-edge-points to the centroids of the surrounding triangles of node *k*. The smoothing domain can be easily extended to 3D problems, where the sub-domain of the smoothing domain for node *k* located in the particular cell j can be obtained by connecting the mid-edge-points, the centroids of the surface triangles and the centroid of cell j. Finding out other sub-domains located in cells which contain node k and the smoothing domain for node k can be constructed by uniting all the sub-domains. Hence, the smoothed strain in 2D using the node-based smoothing technique with triangular element is expressed as

$$\overline{\mathbf{B}}_{\mathrm{I}}^{\text{NS-2D}} = \frac{1}{A^{(k)}} \sum_{j=1}^{N_e^{(k)}} \frac{1}{3} A_e^{(j)} \mathbf{B}_j \tag{27}$$

where $\mathbf{B}_j$ is the compatible strain computed by standard FEM, $\boldsymbol{N}_{\mathrm{e}}$ is the number of elements surrounding the node *k*; A_{e} is the area the *j*th element around the node *k*.

The area $A^{(k)}$ is computed by:

$$A^{(k)} = \int_{\Omega^{(k)}} \mathrm{d}\Omega = \frac{1}{3} \sum_{j=1}^{N_e^{(k)}} A_e^{(j)} \tag{28}$$

Note that with this formulation, only the area and usual “compatible” strain matrices $\mathbf{B}_j$ by Eq. (27) of triangular elements are needed to calculate the system stiffness matrix for the NS-FEM.

In 3D NS-FEM, the smoothed strain can be calculated in a similar way:

$$\overline{\mathbf{B}}_{\mathrm{I}}^{\text{NS-3D}} = \frac{1}{V^{(k)}} \sum_{j=1}^{N_e^{(k)}} \frac{1}{4} V_e^{(j)} \mathbf{B}_j \tag{29}$$

where $\mathbf{B}_j$ is the compatible strain computed by standard FEM, the V_{e} is the volume of the jth tetrahedral element around the node k. The $V_{(k)}$ is computed by:

$$V^{(k)} = \int_{\Omega^{(k)}} \mathrm{d}\Omega = \frac{1}{4} \sum_{j=1}^{N_e^{(k)}} V_e^{(j)} \tag{30}$$

Hence, in the NS-FEM formulation of numerical homogenization, the stiffness matrix and force matrix can be formulated respectively as:

$$\overline{\mathbf{k}}_{\mathrm{NS}} = \sum_{k \in N_e} \int_{\Omega^{(k)}} \left(\mathbf{B}_{\mathrm{NS}}\right)^{\mathrm{T}} \mathbf{D} \mathbf{B}_{\mathrm{NS}} d\Omega \tag{31}$$

$$\overline{\mathbf{F}}_{\mathrm{NS}} = \sum_{k \in N_e} \int_{\Omega^{(k)}} \left(\mathbf{B}_{\mathrm{NS}}\right)^{\mathrm{T}} \mathbf{D} d\Omega \tag{32}$$

In the formulation of multi-material NS-FEM, the smoothing domain is also separated two parts along the interface of different material as shown in Fig. 3(b) as material properties are not continuous. That means the associated smoothing domain is not allowed to cross the boundary of each material. It is noted that there are still some smoothing effect at both sides of interface, but smoothing effect is weak compared with internal nodes.

3.3 Cell-based smoothed finite element method

In the cell-based smoothed finite element method (CS-FEM) for the homogenization, the quadrilateral elements are considered. The formulation of stiffness is computed based on the smoothing cells (SC) located inside the quadrilateral elements as shown in Fig. 5. In CS-FEM, the elements are subdivided into several smoothing cells, such as $\Omega^e = \Omega_1^e \cup \Omega_1^e \cup ...\Omega_{nc}^e$. If the number of SC of the elements equals 1, the CS-FEM solution has the same properties with those of standard FEM using the reduced integration [24]. When the number of smoothing cells is approaching infinity, the CS-FEM solution approaches to the solution of standard FEM. Based on our research experience, the numerical solution is always stable and accurate if the number of smoothing cells is equal to 4 [24].

Based on the smoothing theory, the smoothed strain in CS-FEM can be expressed in the following equation:

$$\bar{\boldsymbol{\varepsilon}}_{\mathrm{CS}} = \sum_I^n \bar{\mathbf{B}}_{\mathrm{CS}}\left(\mathbf{x}_C\right)\mathbf{u}_I \tag{33}$$

where $\bar{\mathbf{B}}_{\mathrm{CS}}$ is the smoothed strain matrix. For 2D case

$$\bar{\mathbf{B}}_{\mathrm{CS}} = \begin{bmatrix} \bar{b}_{\mathrm{CS}} & 0 \\ 0 & \bar{b}_{\mathrm{CS}} \\ \bar{b}_{\mathrm{CS}} & \bar{b}_{\mathrm{CS}} \end{bmatrix} \tag{34}$$

where

$$\bar{b}_{CS} = \frac{1}{A_C}\int_{\Gamma_c} N_I\left(\mathbf{x}\right) n_k\left(\mathbf{x}\right) d\Gamma \tag{35}$$

If one Gaussian point is used for line integration along each segment of boundary Γ_i^C of Ω_C, the above integration equation can be transformed to its algebraic form

$$\bar{b}_{CS} = \sum_{i=1}^{M} N_I\left(\mathbf{x}_i^{\mathrm{GP}}\right) n_{ik}^{C} l_{ik}^{C} \tag{36}$$

where $\mathbf{x}_i^{\mathrm{GP}}$ is the midpoint (Gaussian point) of boundary segment of Γ_i^C, whose length and outward unit normal are denoted as l_i^C and n_i^C , respectively.

The smoothed element stiffness matrix can be obtained by assembly of those all of the smoothing cells of the element, i.e.

$$\overline{\mathbf{K}}_{\mathrm{CS}} = \sum_{C} \overline{\mathbf{B}}_{\mathrm{CS}}^{\mathrm{T}} \mathbf{D} \mathbf{B}_{\mathrm{CS}} A_{\mathrm{CS}} \tag{37}$$

$$\overline{\mathbf{F}}_{\mathrm{CS}} = \sum_{C} \overline{\mathbf{B}}_{\mathrm{CS}}^{\mathrm{T}} \mathbf{D} A_{\mathrm{CS}} \tag{38}$$

The smoothed $\overline{\mathbf{B}}_{\mathrm{CS}}$ matrices are constructed with integration over the boundary of the cell of the element.

3.4. Algorithm for S-FEMs based homogenization

Numerical procedures for computing the effective mechanical properties of composite materials using smoothed finite element method are summarized as follows:

1. Design Composite material

2. Determine the unit cell

3. Divide the domain into a set of elements and obtain information on nodes coordinates and element connectivity

4. Create the smoothing domain for each smoothed finite element method.

5. Loop over all the elements

(a) Compute the compatible strain **B** of the element by Equation using standard finite element formulation and save it to process the smoothed strain.

(b) Evaluate the smoothed strain. In ES-FEM, apply Eq. (22) and (23) to compute the edge-based smoothed strain. In NS-FEM, use Eq. (27) and (29) to calculate the node-based smoothed strain. In CS-FEM, Eq. (34) is adopted to determine the cell-based smoothed strain.

6. Calculation of smoothed stiffness and smoothed force matrix

- For ES-FEM, smoothed stiffness and force in numerical homogenization use Eq. (25) and (26)
- For NS-FEM, smoothed stiffness and force in numerical homogenization use Eq. (31) and (32)
- For CS-FEM, smoothed stiffness and force in numerical homogenization use Eq. (37) and (38)

7. Implement symmetrical boundary conditions by referring to Table 1 and 2.

8. Solve homogenization equation $\overline{\mathbf{K}}\mathbf{d}^{n} = \overline{\mathbf{F}}^{n}$

9. Evaluate the homogenized (effective) mechanical properties based on Eq. (13).

10. For 2D elasticity problem, loop step 7 and 8 three times for different boundary conditions. For 3D elasticity problem, repeat the step 7 and 8 six times for different characterized cases.

4. Numerical examples

4.1 Benchmark example

In order to verify the S-FEMs formulation for homogenization, one benchmark example [9] is first studied. As shown in Fig. 6, unit square cell containing a 0.4×0.6 void and the solid phase material properties are D_{11}=D_{22}=30 and D_{12}=D_{33}=10 (all units are assumed to be consistent) [9]. This problem was solved by Bendsoe and Kikuchi [16].

The numerical solutions obtained from S-FEMs and FEM using the triangular (T3) and quadrilateral (Q4) elements (Fig. 7) are tabulated in Tables 3 and 4, respectively. For the purpose of comparison, the published results are presented in Table 5. Compared these three tables, it is seen the homogenization results obtained from S-FEMs agree very well with the published data.

4.2 Void material

Another example is material 1 with void as shown in Fig. 8. The Young modulus and Poisson's ratio of solid are E=5MPa, v=0.3. A plane stress problem is considered here. The discretized models using triangular (T3) and quadrilateral (Q4) elements are shown in Fig. 9.

Figure 10 shows the convergence of effective (homogenized) bulk modulus using different FEM methods. The effective bulk modulus is defined by [40]:

$$Bu = \frac{E_{eff}}{2(1-v_{eff})} = \frac{E_{eff}}{4(1-v_{eff}^2)}\left(2+2v_{eff}\right) = \frac{1}{4}\left(D_{11}^{eff} + 2D_{12}^{eff} + D_{22}^{eff}\right) \tag{39}$$

The effective elasticity tensor $\mathbf{D}^{eff}$ can be defined as follows:

2D plan stress problem

$$\mathbf{D}^{eff} = \frac{E_{eff}}{1-v_{eff}^2}\begin{bmatrix} 1 & v_{eff} & 0 \\ v_{eff} & 1 & 0 \\ 0 & 0 & \left(1-v_{eff}\right)/2 \end{bmatrix} = \begin{bmatrix} D_{1111}^{eff} & D_{1122}^{eff} & 0 \\ D_{1122}^{eff} & D_{2222}^{eff} & 0 \\ 0 & 0 & D_{1212}^{eff} \end{bmatrix} \tag{40}$$

2D plan stain problem

$$\mathbf{D}^{eff} = \frac{E_{eff}}{\left(1+v_{eff}\right)\times\left(1-2v_{eff}\right)}\begin{bmatrix} 1-v_{eff} & v_{eff} & 0 \\ v_{eff} & 1-v_{eff} & 0 \\ 0 & 0 & \left(1-2v_{eff}\right)/2 \end{bmatrix} = \begin{bmatrix} D_{1111}^{eff} & D_{1122}^{eff} & 0 \\ D_{1122}^{eff} & D_{2222}^{eff} & 0 \\ 0 & 0 & D_{1212}^{eff} \end{bmatrix} \tag{41}$$

where E_{eff} is effective Young Modulus and v_{eff} is effective Poisson's ratio. The short notation $\mathbf{D}_{ijkl}^{eff}$ ($11 \leftrightarrow 1, 22 \leftrightarrow 2, 33 \leftrightarrow 3, 32 \leftrightarrow 4, 13 \text{ or } 31 \leftrightarrow 5, 12 \text{ or } 21 \leftrightarrow 6$) is used for all the entries of the homogenized effective elasticity tensor [40].

In order to make a comparison, the reference solution is computed using standard FEM with very fine mesh (35621 nodes). As shown in Fig. 10, it is seen that all numerical results approach the reference solution with increased number of degree of freedom (DOF). The FEM, ES-FEM and CS-FEM approach the reference solution from the upper bound, whereas NS-FEM with T3 and Q4 elements approaches the reference solution from the lower side. Among all numerical methods, ES-FEM gives the most accurate solution even much better than quadrilateral (Q4) elements using FEM, which is due to stronger softening effect provided by the ES-FEM.

4.2 Multiple material composites

In this section, two different materials with void are bonded together as shown in Fig. 11. The Young moduli for materials 1 and 2 re E_1=0.1GPa and E_2=2GPa, Poisson's ratios for materials 1 and 2 are v_1=0.4 and v_2=0.3, respectively. Plane strain problem is considered here.

By using the same set of T3 meshes as shown in Fig. 12, Fig. 13 plots the convergence in the effective (homogenized) elasticity components using the different finite element methods. The solutions of all these methods converge to the reference solution (36260 nodes using FEM) with reducing nodal spacing. In terms of the accuracy, the NS-FEM gives similar results to FEM. However, NS-FEM converges the reference solution from the lower bound, whilst FEM converges the reference solution from the upper bound. Among all numerical methods, again ES-FEM provides the best solution in all elasticity components.

Figure 14 outlines the converegcne of effective (homogenized) bulk modulus. It is observed that numerical solution obtained from ES-FEM is again the closest to the reference solution when the same set of mesh is used.

As computational efficiency is an important criterion to assess the performance of numerical methods, the comparison of different analysis methods is shown in Fig. 15. It is clear that the computational time for the ES-FEM and NS-FEM is longer than FEM when the same set of mesh is used. This is because more nodes are used to form the shape function in ES-FEM and NS-FEM. Nevertheless, in terms of computational efficiency, the ES-FEM performs much better than FEM and NS-FEM. This is due to right softened effect in the ES-FEM model.

Another example of numerical homogenization for multi-phase material is shown in Fig. 16. The Young modulus for material 1 and 2 are $E_1 = 200\text{MPa}$ and $E_2 = 30\text{MPa}$, Poisson's ratio for material 1 and 2 are $v_1 = 0.3$ and $v_2 = 0.35$ respectively. The discretization model is shown in Fig. 17.

The convergence rates of effective mechanical properties are presented with different numerical methods shown in Fig. 18. From Fig. 18, again we found that the ES-FEM gives much better solution than FEM and NS-FEM. Fig. 19 plots the result of effective bulk modulus converging to the reference solution using different methods. As we expected, FEM and ES-FEM give upper bound solution and NS-FEM provides lower bound solution. The ES-FEM is able to achieve a close to exact stiffness, and it gives the best solution in the prediction of effective bulk modulus.

4.3 Tissue Scaffold Example

As the rapid development of additive fabrication technology, scaffold tissue engineering is growing fast. Materials with periodic cellular micro-architectures are becoming particularly advantageous due to high manufacturability and tailored effective properties. Tissue scaffold involves two important criteria concerned in the design stage: one is overall stiffness, which is able to provide similar load-bearing capacities to surrounding tissues; the other one is permeability, which offers sufficient porosity for mass transfer and vascularization. In this example, it is assumed that the Young modulus E=100Mpa, $\nu = 0.3$ of scaffold materials the permeability coefficient $\kappa = 0.5$ in the 3D tissue scaffold as shown in Fig. 20.

The discretization of 3D base cell is presented in Fig. 21. Fig. 22 shows the convergence of effective bulk modulus using 3D ES-FEM, NS-FEM and FEM. In order to make a comparison, the reference solution with very fine mesh (216,000 nodes) is also plotted together. It is clearly shown that 3D ES-FEM still gives the best solution of these different numerical methods when the same set of mesh is used. The 3D NS-FEM still approaches the reference solution from the lower bound.

The convergence of effective permeability is presented in Fig. 23 with reference solution using 216,000 nodes. Again, it is found the NS-FEM provides the lower bound solution of effective permeability. The ES-FEM and FEM provides the upper bound solution of effective permeability. In terms of accuracy, the ES-FEM using tetrahedral (T4) elements performs the best.

5. Conclusion

In this paper, smoothed finite element methods (S-FEMs) were formulated to solve the numerical homogenization problems. Various 2D and 3D examples were presented to demonstrate the accuracy and convergence of S-FEMs in the evaluation of effective (homogenized) mechanical properties of periodic microstructural composites. In summary, some conclusions are drawn as follows:

1. The implementation of smoothed finite element method in numerical homogenization of composite material is fairly straightforward. No additional parameters are involved in the formulation.
2. For the first time, the NS-FEM was found to be able to give the lower bound solution in the computation of effective (homogenized) material properties of composites.
3. The ES-FEM was found to stand out from all different forms of finite element method in 2D and 3D, which provided the best solution to characterization of the effective mechanical properties of composites.

Reference

[1] Boso DP, Lefik M, Schrefler BA, Recent developments in numerical homogenization. Computer Assisted Mechanics and Engineering Sciences, 2009; 16: 161–183.

[2] Zhou SW, Li Q, A microstructure diagram for known bounds in conductivity. Journal of Materials Research, 2008; 23(3) 798-811.

[3] Hashin, Z, Shtrikman S, A variational approach to the theory of composite elastic materials. Journal of the mechanics and physics of solids, 1963; 11(2): 127-140.

[4] Berryman JG, Milton GW, Microgeometry of random composites and porous-media. Journal of Physics D-Applied Physics, 1988; 21(1) : p87-97.

[5] Cherkaev AV, Gibiansky LV, coupled estimates for the bulk and shear moduli of a 2-dimensional isotropic elastic composite. Journal of the mechanics and physics of solids, 1993; 41(5): 937-980.

[6]Ye Z, Yu W, A New Approach to Bounding Effective Properties of Random Heterogeneous Materials. 52nd AIAA/ASME/ASCE/AHS/ASC Structures, Structural Dynamics and Materials Conference.

[7] Hollister SJ, Kikuchi N, A Comparison of Homogenization and Standard Mechanics Analyses for Periodic Porous Composites. Computational Mechanics, 1992; 10: 73 – 95.

[8] Hassani B, Hinton E, A Review of Homogenization and Topology Optimization I – Homogenization Theory for Media with Periodic Structure. Computer & Structures, 1998: 69: 707 – 717.

[9] Hassani B, Hinton E, A Review of Homogenization and Topology Optimization II – Analytical and Numerical Solution of Homogenization Equations. Computer & Structures, 1998; 69: 719 – 738.

[10] Sun H, Di S, Zhang N, Wu C, Micromechanics of Composite Materials using Multivariable Finite Element Method and Homogenization Theory. International Journal of Solids and Structures, 2001; 38: 3007 – 3020.

[11] Alexander A, Tzeng JT, Three Dimensional Effective Properties of Composite Materials for Finite Element Applications, Journal of Composite Materials, 1997; 31(5): 466-485.

[12] Guedes JM, Kikuchi N, Preprocessing and postprocessing for materials based on the homogenization method with adaptive finite element method. Computer methods in applied mechanics and engineering, 1990; 83: 143-198.

[13] Yi Y, Park S, Youn S, Asymptotic Homogenization of Viscoelastic Composites with Periodic Microstructures. International Journal of Solids and Structures, 1998; 35: 2039 – 2055.

[14] Fujii D, Chen BC, Kikuchi N, Composite material design of two-dimensional structures using the homogenization design method. International Journal for Numerical Methods in Engineering, 2001; 50: 2031-2051.

[15] Fang Z, Sun W, Tzeng JT, Asymptotic Homogenization and Numerical implementation to Predict the Effective Mechanical Properties for Electromagnetic Composite Conductor. Journal of Composite Materials, 2004; 38: 1371.

[16] Bendsoe MP, Kikuchi N, Generating optimal topologies in structural design using a homogenization method. Computer methods in applied mechanics and engineering, 1988; 71: 197-224.

[17] Michel JC, Moulinec H, Suquet P, Effective properties of composite materials with periodic microstructure: a computational approach. Computer methods in applied mechanics and engineering, 1999; 172: 109-143.

[18] Andreassen E, Andreasen CS, How to determine composite material properties using numerical homogenization. Computational Materials Science, 2014; 83: 488 – 495.

[19] Zienkiewicz OC, Taylor RL. The Finite Element Method (5th edn). Butterworth Heinemann: Oxford, U.K., 2000.

[20] Liu GR, Meshfree methods: Moving beyond the Finite Element Method. CRC Press: Boca Raton, U.S.A, 2002.

[21] Liu GR, A G space theory and a weakened weak (W2) form for a unified formulation of compatible and incompatible methods: Part I theory. International Journal for Numerical Methods in Engineering, 2010; 81: 1093-1126.

[22] Liu GR, Zhang GY. Smoothed Point Interpolation Methods. Singapore: World Scientific, 2013.

[23] Chen JS, Wu CT, Yoon S, You Y, A stabilized conforming nodal integration for Galerkin mesh-free methods, International Journal for Numerical Methods in Engineering, 2001; 50: 435–466.

[24] Liu GR, Dai KY, Nguyen TT, A smoothed finite element method for mechanics problems, Computational Mechanics, 2007; 39: 859 – 77.

[25] Liu GR, Nguyen TT, Dai KY, Lam KY, Theoretical aspects of the smoothed finite element method (SFEM). International Journal for Numerical Methods in Engineering, 2007; 71: 902 – 30.

[26] Liu GR, Nguyen-Thoi T, Dai KY, Lam KY, Theoretical aspects of the smoothed finite element method (SFEM). International Journal for Numerical Methods in Engineering, 2007; 71: 902–930.

[27] Hung NX, Bordas S, Hung N-D, Smooth finite element methods: convergence, accuracy and properties. International Journal for Numerical Methods in Engineering, 2008; 74: 175–208.

[28] Liu GR, Nguyen TT, Nguyen HX, Lam KY, A node-based smoothed finite element method (NS-FEM) for upper bound solutions to solid mechanics problems. Computers and Structures, 2009; 87: 14-26.

[29] Liu GR, Nguyen-Thoi T, Lam KY, An edge-based smoothed finite element method (ES-FEM) for static, free and forced vibration analyses of solids. Journal of Sound and Vibration. 2009; 320: 1100–1130.

[30] He ZC, Li GY, Zhong ZH, Cheng AG, Zhang GY, Li E, Liu GR, An ES-FEM for accurate analysis of 3D mid-frequency acoustics using tetrahedron mesh. Computers and Structures, 2012; 106-107: 125-134.

[31] He ZC, Li GY, Zhong ZH, Cheng AG, Zhang GY, Liu GR, Li E, Zhou Z, An edge-based smoothed tetrahedron finite element method (ES-T-FEM) for 3D static and dynamic problems. Computational mechanics, 2013; 2:221-236.

[32] Li E, Liu GR, Tan V, and He ZC, Modeling and simulation of bioheat transfer in the human eye using the 3D alpha finite element method (αFEM). Intentional Journal for Numerical Methods in Biomedical Engineering, 2010; 26: 955–976.

[33] Li E, Liu GR, Tan V, Simulation of Hyperthermia Treatment Using the Edge-Based Smoothed Finite-Element Method. Numerical Heat Transfer, Part A: Applications, 2010; 57(11): 822 -847.

[34] Li E, Liu GR, Tan V, and He ZC, An efficient algorithm for phase change problem in tumor treatment using αFEM. International Journal of Thermal Sciences, 2010; 49 (10): 1954-1967.

[35] Li E, He ZC, Xu X, A novel edge-based smoothed tetrahedron finite element method (ES-T-FEM) for thermomechanical problems. International Journal of Heat and Mass Transfer, 2013; 66: 723 – 732.

[36] He ZC, Cheng AG, Zhong ZH, Zhang GY, Li GY, Li E, An improved eigenfrequencies prediction for three-dimensional problems using face-based smoothed finite element method. Journal of Acta Mechanica Solida Sinica, 2013; 26: 140-150.

[37] He ZC, Li GY, Li E, Zhong ZH, Liu GR, Mid-frequency acoustics analysis using edge-based smoothed tetrahedron radial point interpolation method (ES-T-RPIM). Submitted to Computational methods. 2013 (Accepted).

[38] Kuznetsov S. Homogenization Methods for Problems with Multiphysics, Temporal and Spatial Coupling. PhD thesis. Columbia University 2012.

[39] Liu GR. A generalized gradient smoothing technique and the smoothed bilinear form for Galerkin formulation of a wide class of computational methods. International Journal of Computational Methods, 2008; 5:199 – 236.

[40] Kruijf ND, Zhou SH, Li Q, Mai YW, Topological design of structures and composite materials with multiobjectives. International Journal of Solids and Structures, 2007; 44: 7092-7109.

Figure

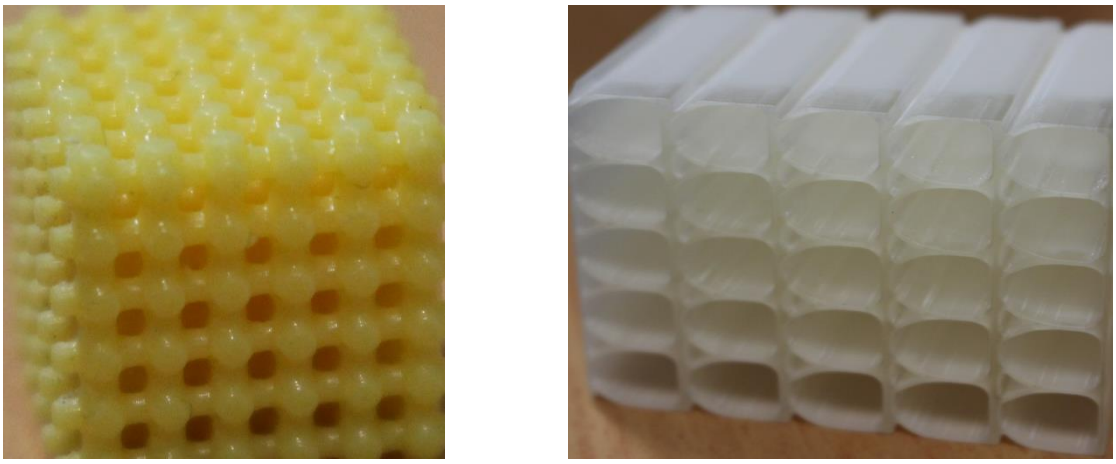

(a) Tissue Scaffold (b) Cuttlebone

Figure 1: 3D printing of composite material

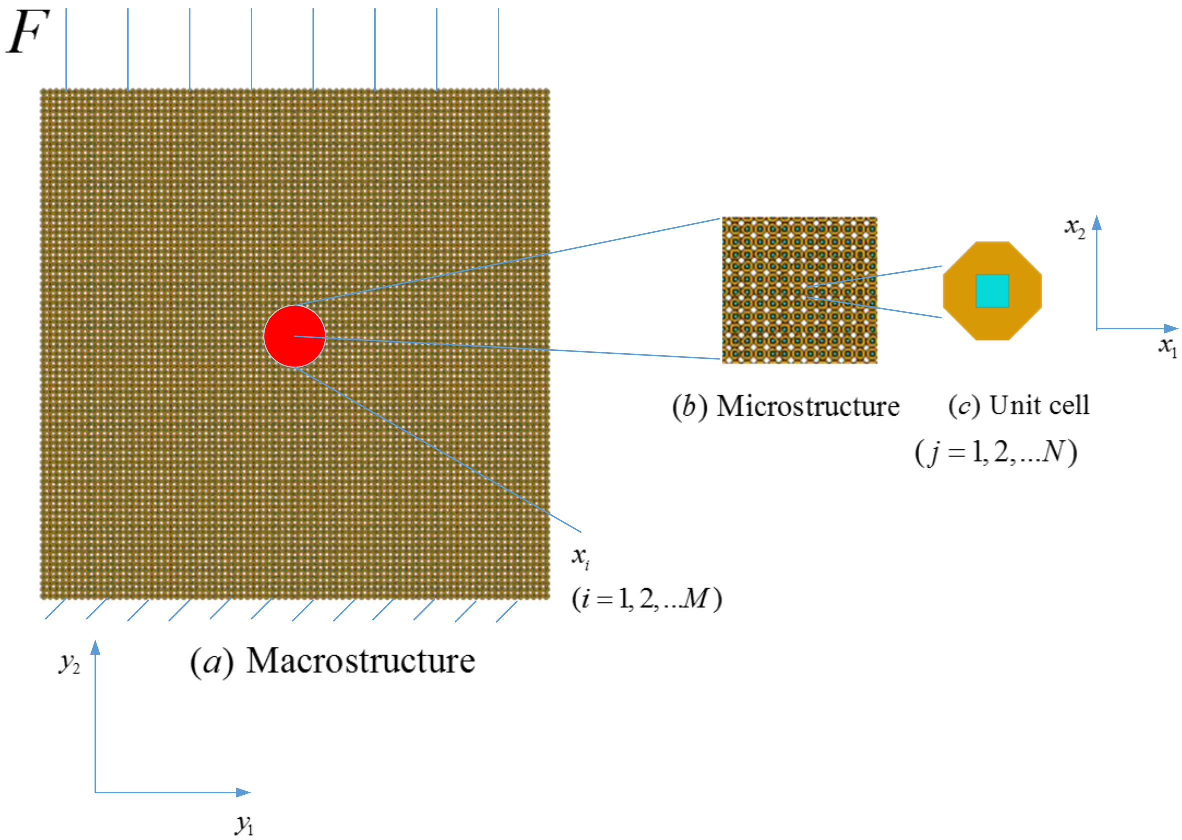

Figure 2: Composite materials with periodic microstructure

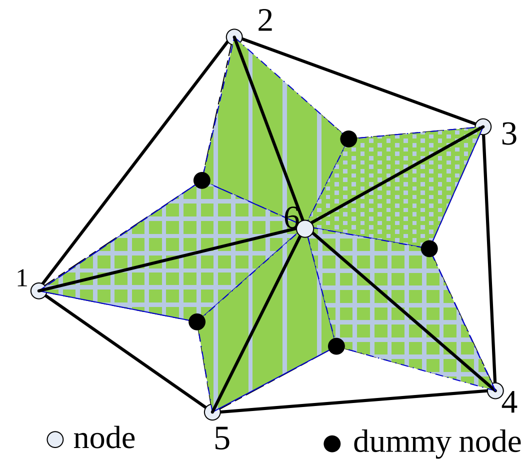

a) Single material

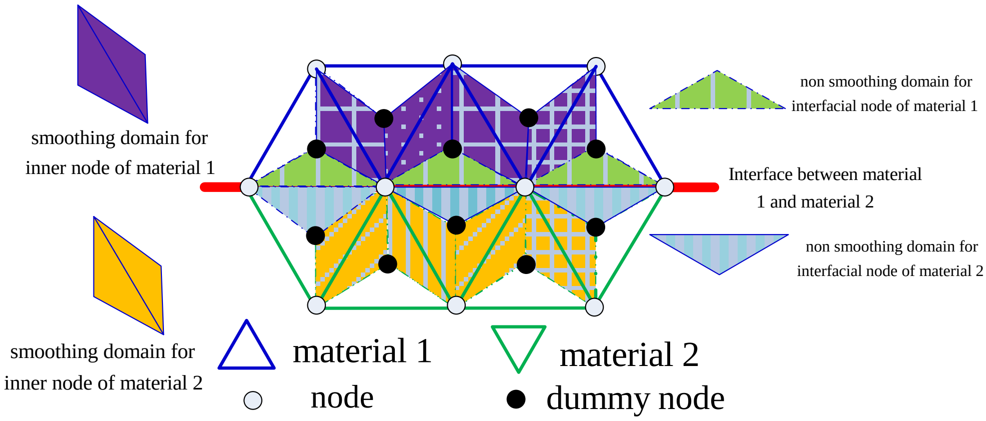

b) Multi-material

Figure 3: Illustration of ES-FEM

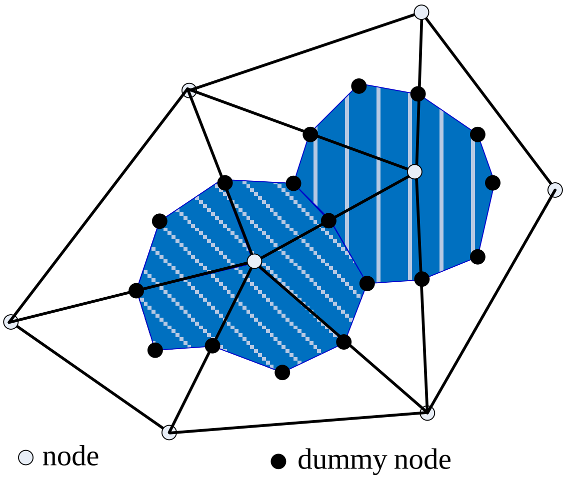

a) Single material

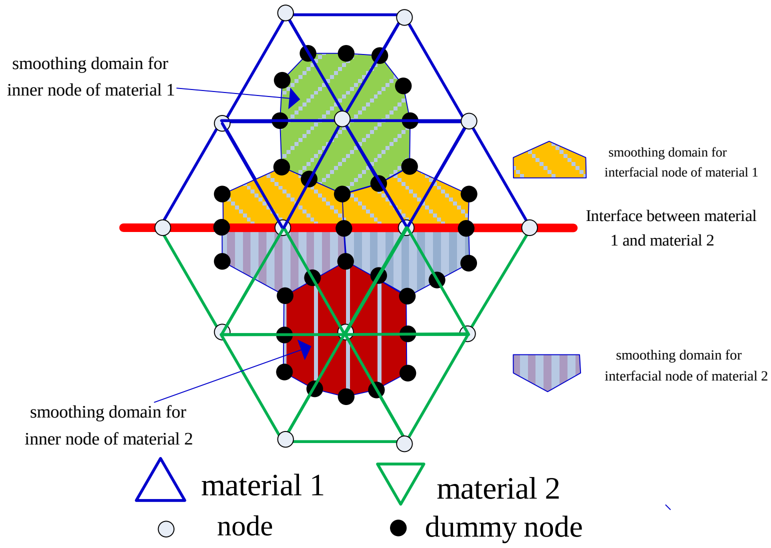

b) Multi-material

Figure 4: Illustration of NS-FEM

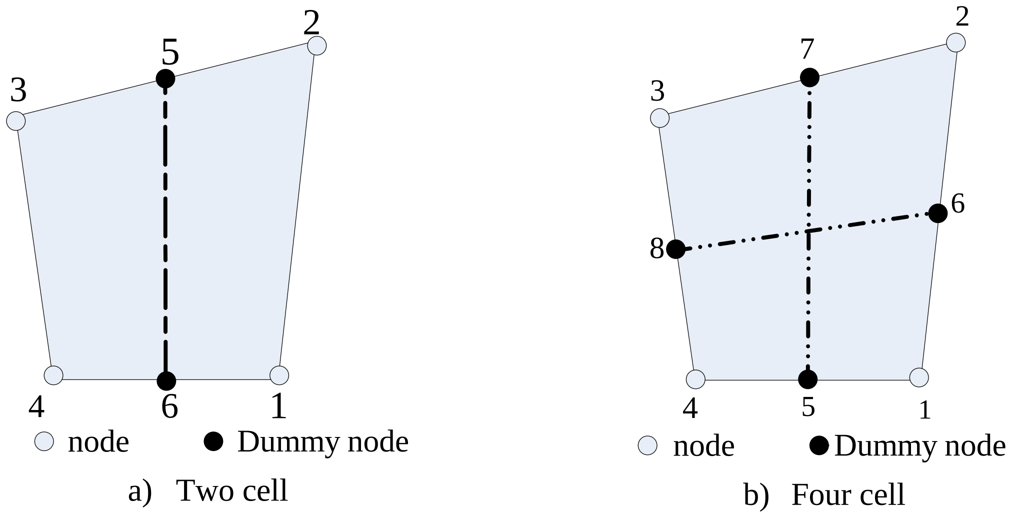

Figure 5: Illustration of CS-FEM

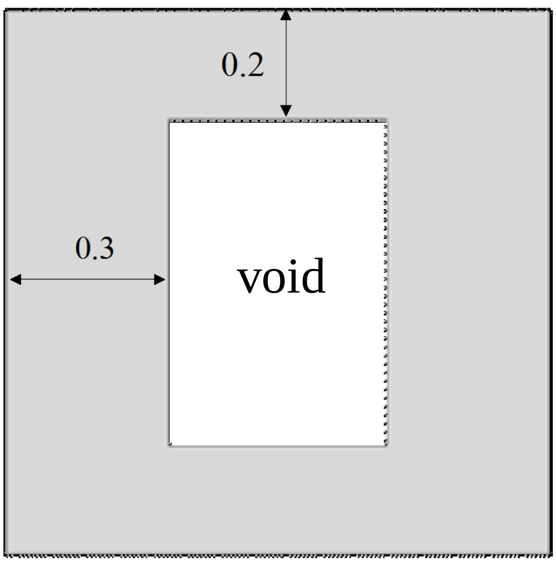

Figure 6: Unit cell of a periodic composite

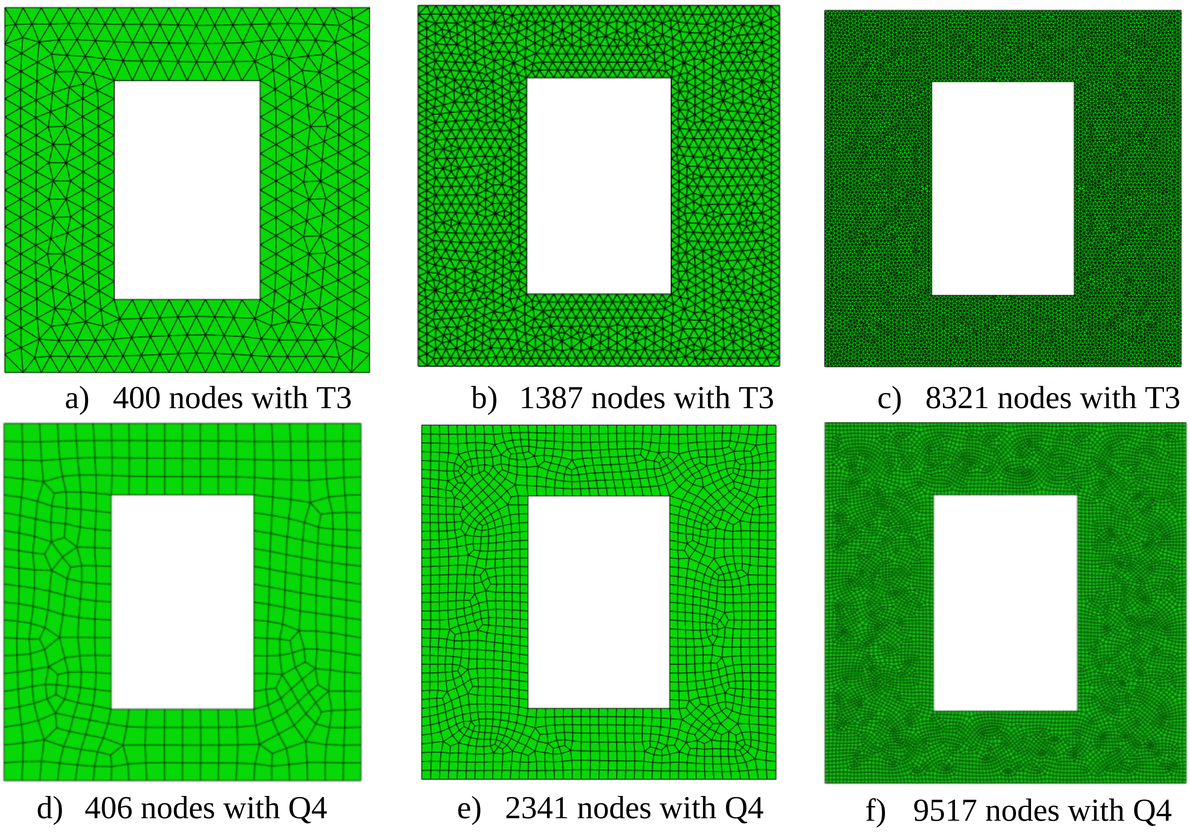

Figure 7: Discretization of base cell using triangular (T3) and quadrilateral (Q4) elements

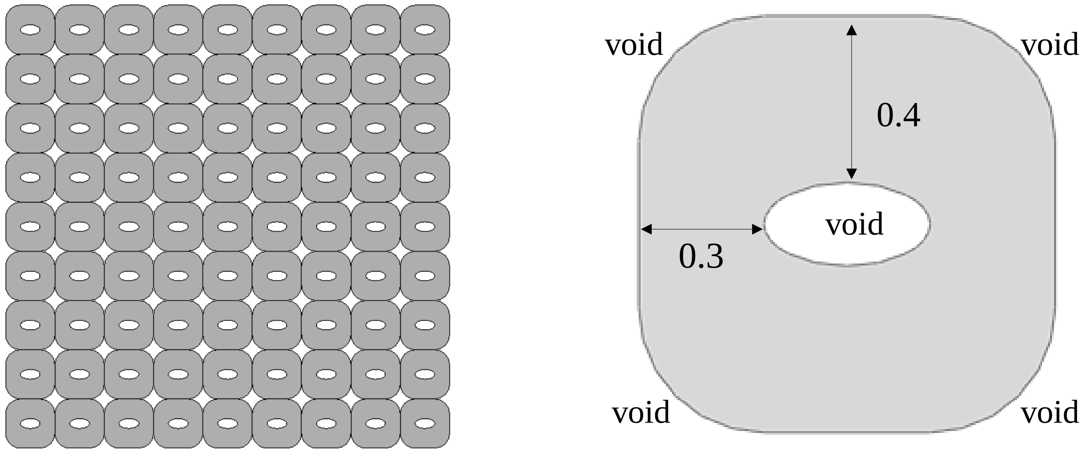

a) Periodic structure b) RVE

Figure 8: Base cell of a composite

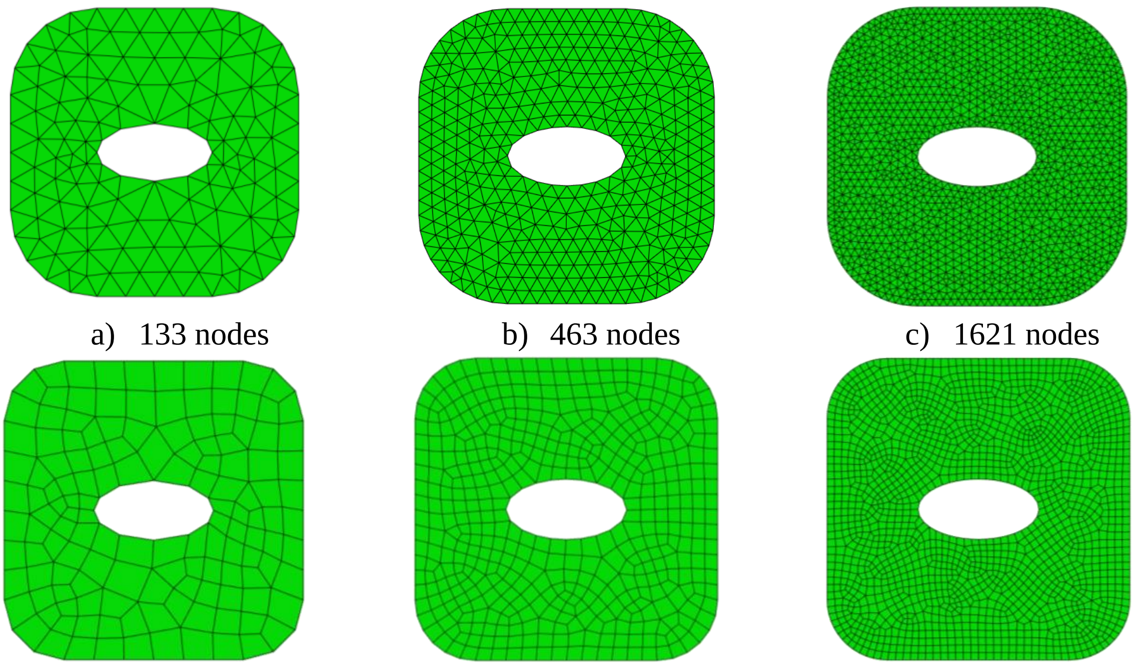

a) 133 nodes b) 463 nodes c) 1621 nodes

d) 162 nodes e) 521 nodes f) 1837 nodes

Figure 9:Domain discretization using triangular and quadrilateral element

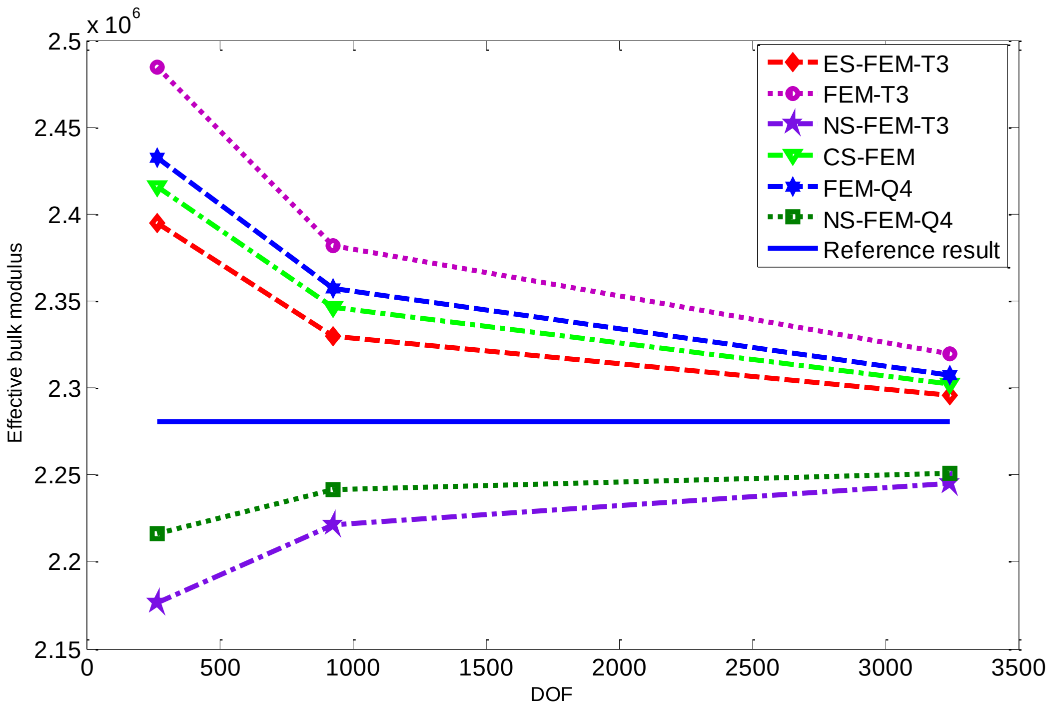

Figure 10: Convergence of bulk modulus

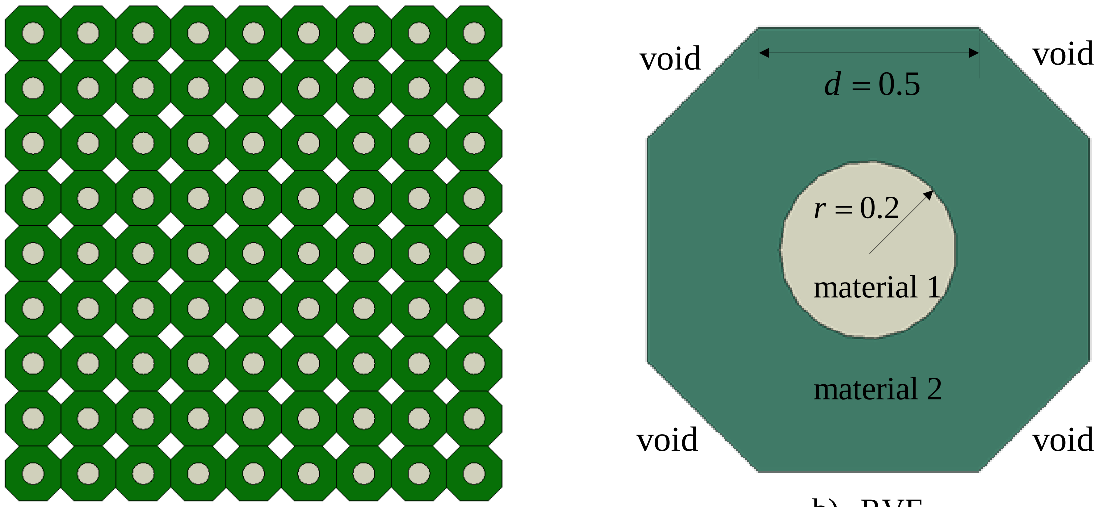

a) Periodic structure

b) RVE

Figure 11: Base cell of a composite

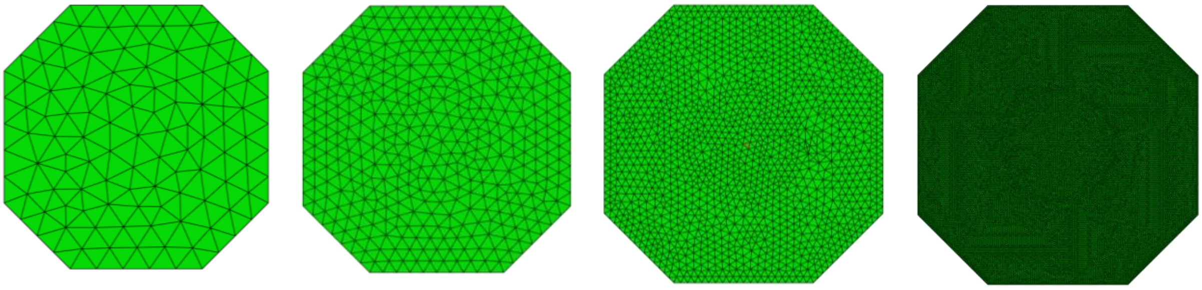

(a)122 nodes (b) 417 nodes (b) 1445 nodes (d) 36260 nodes

Figure 12: Domain discretization using triangular (T3) element

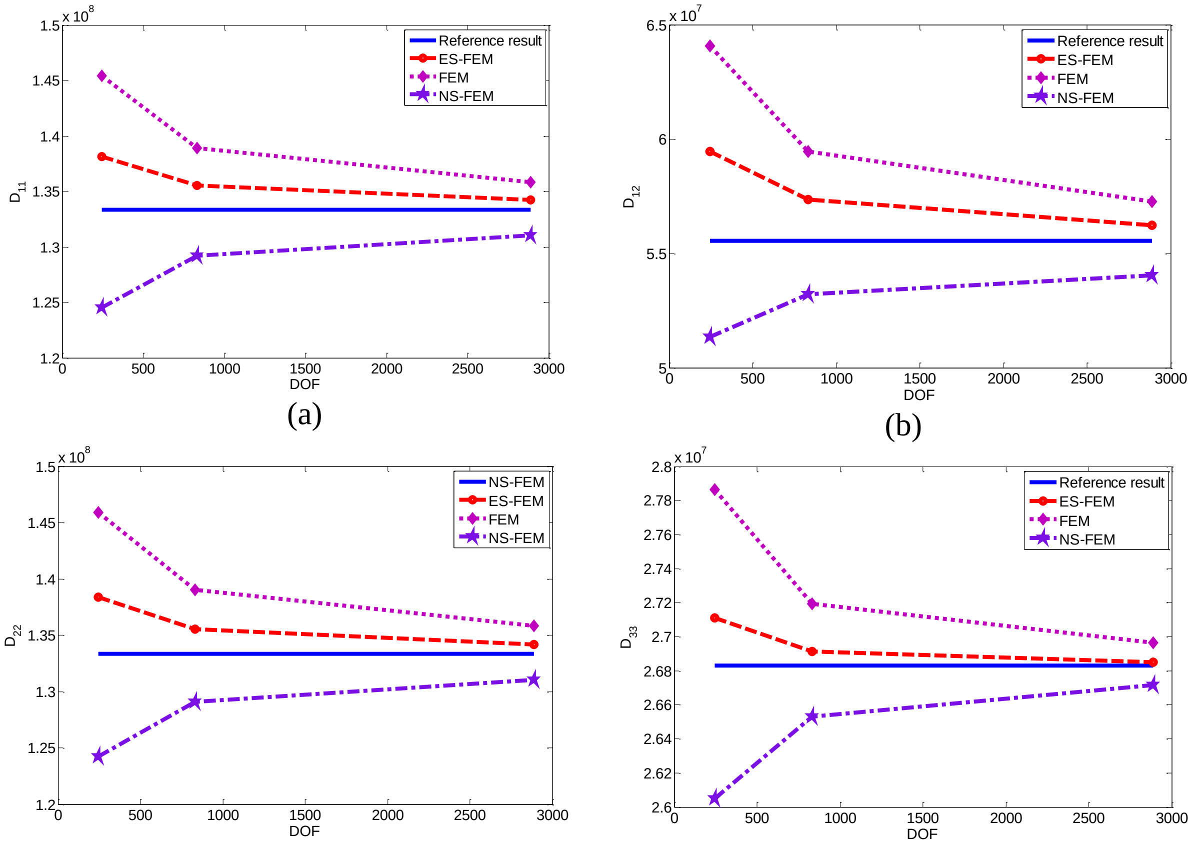

(a) (b) (c) (d)

Figure 13:Convergence of elasticity components

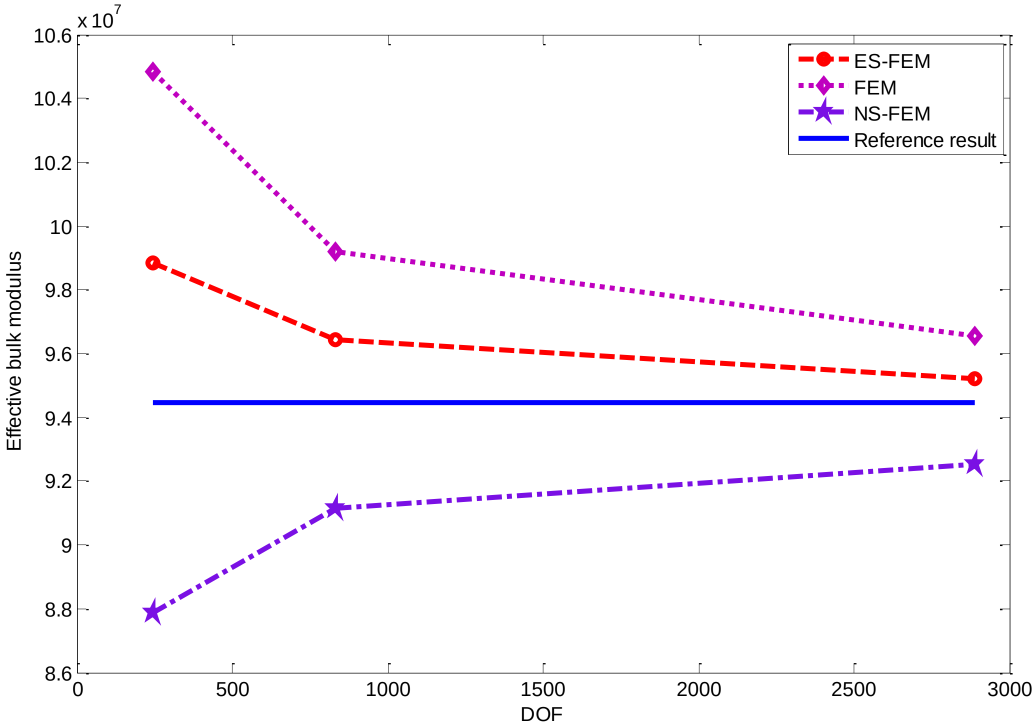

Figure 14: Convergence of effective bulk modulus

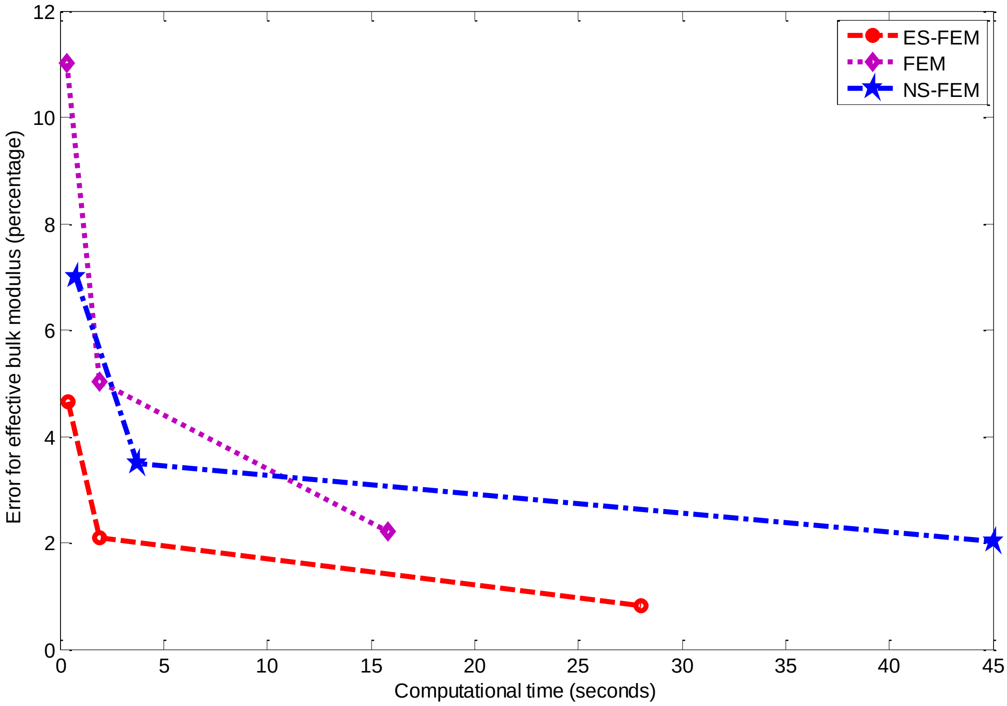

Figure 15: Convergence of effective bulk modulus

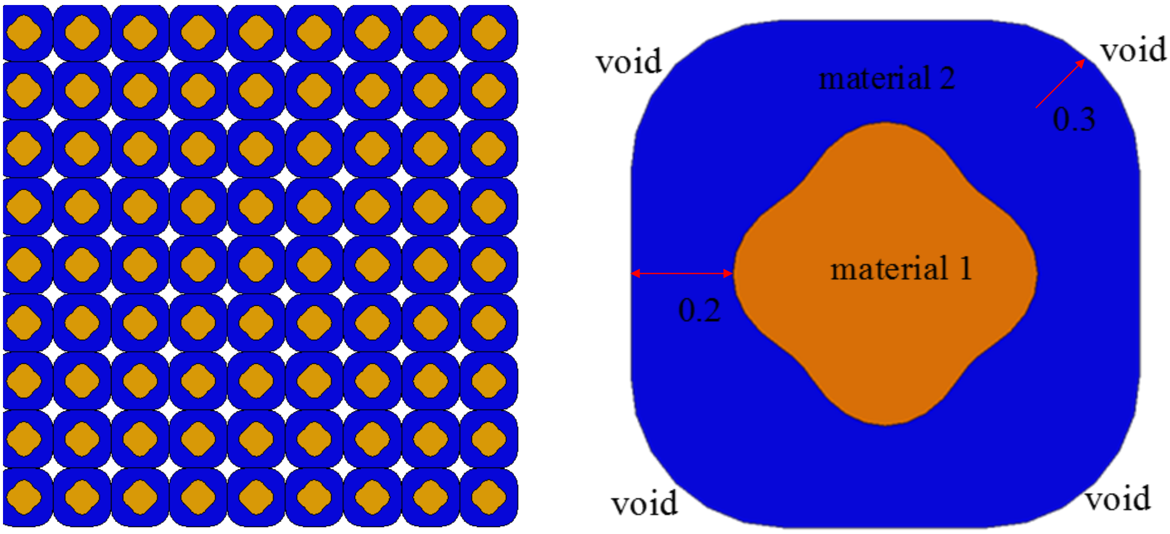

a) Periodic structure b) RVE

Figure 16: Base cell of a composite

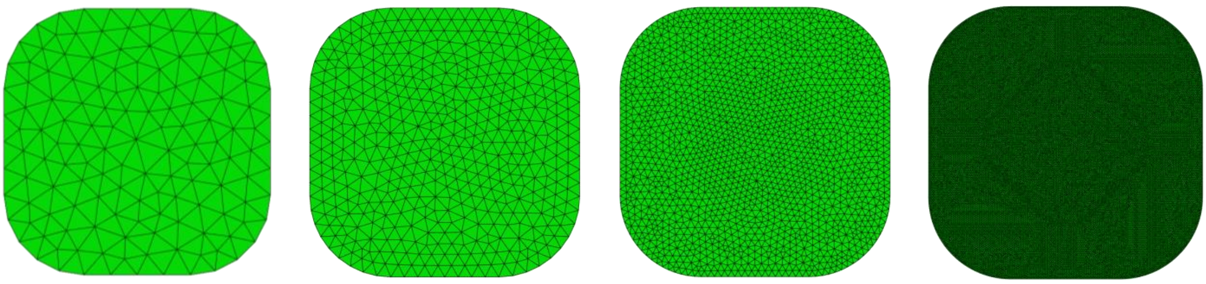

(a)145 nodes (b) 501 nodes (b) 1756 nodes (d) 38685 nodes

Figure 17: Domain discretization using triangular element

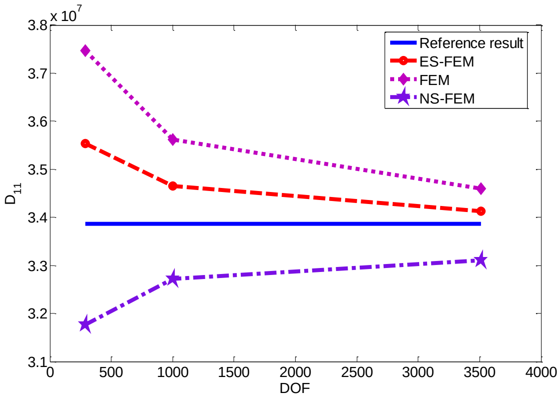

(b)

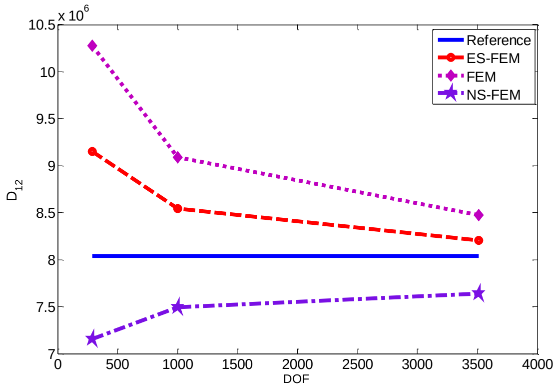

(b)

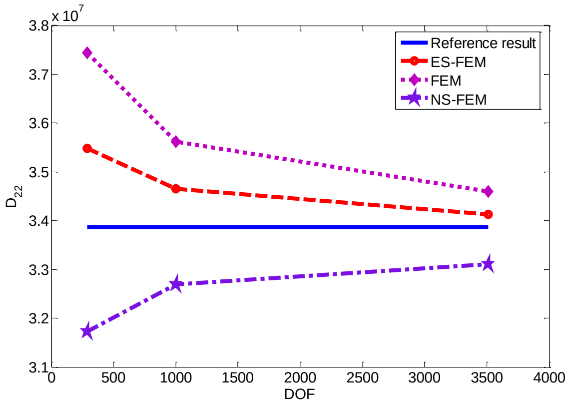

(c)

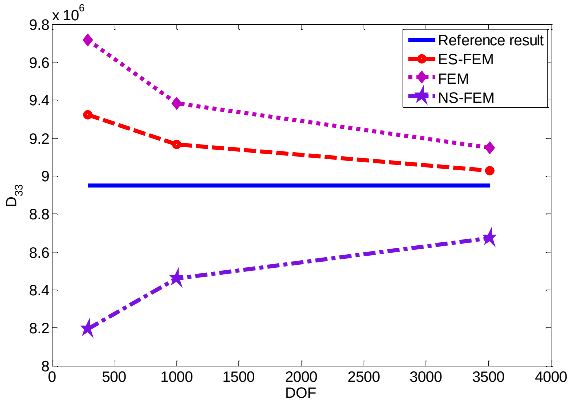

(d)

Figure 18:Convergence of bulk modulus

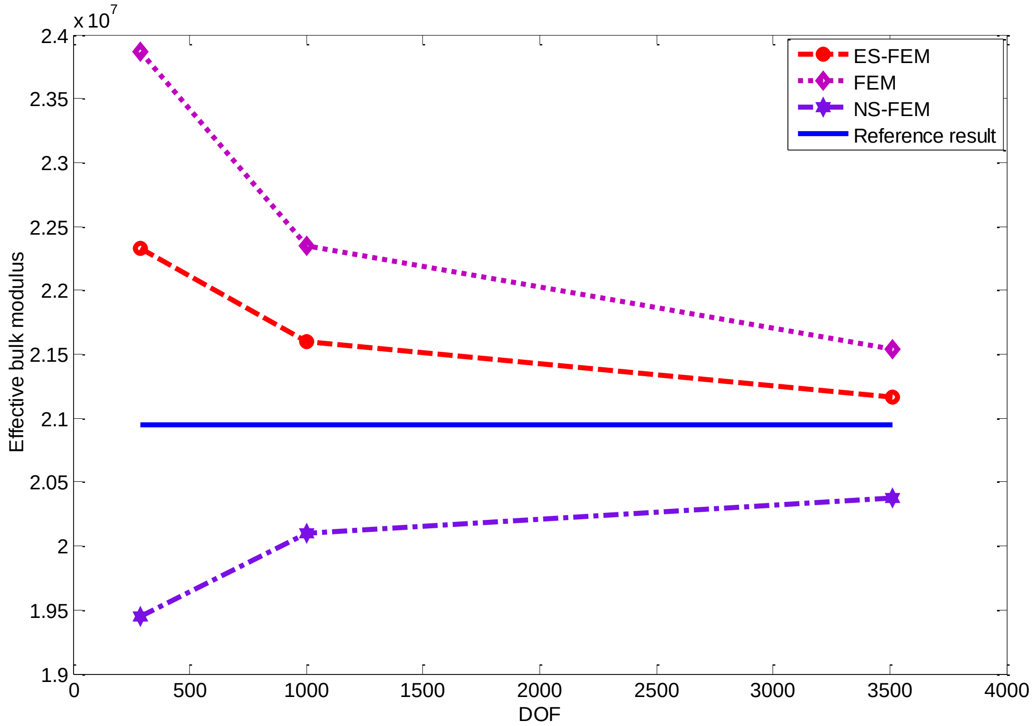

Figure 19: Convergence of bulk modulus

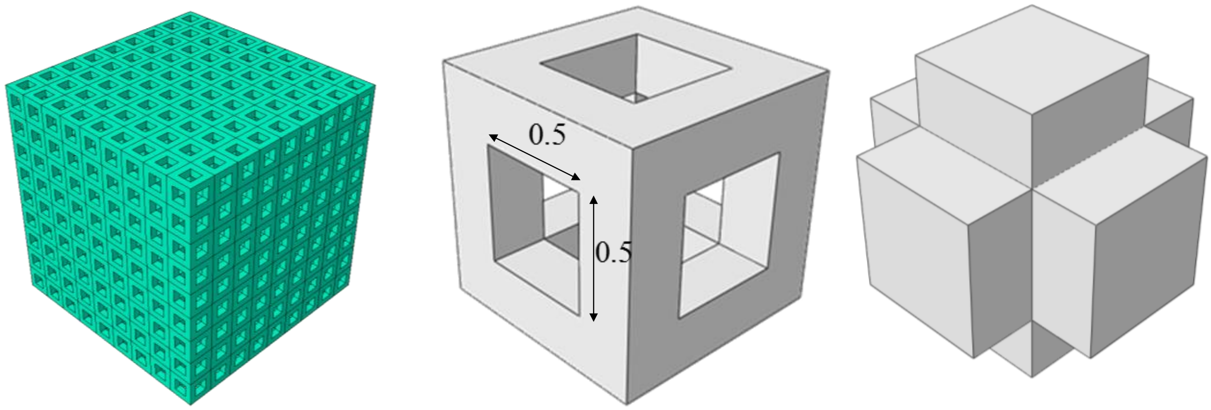

a) 3D tissue Scaffold b) RVE for stiffness model c) RVE for Permeability model

Figure 20: 3D tissue scaffold structure

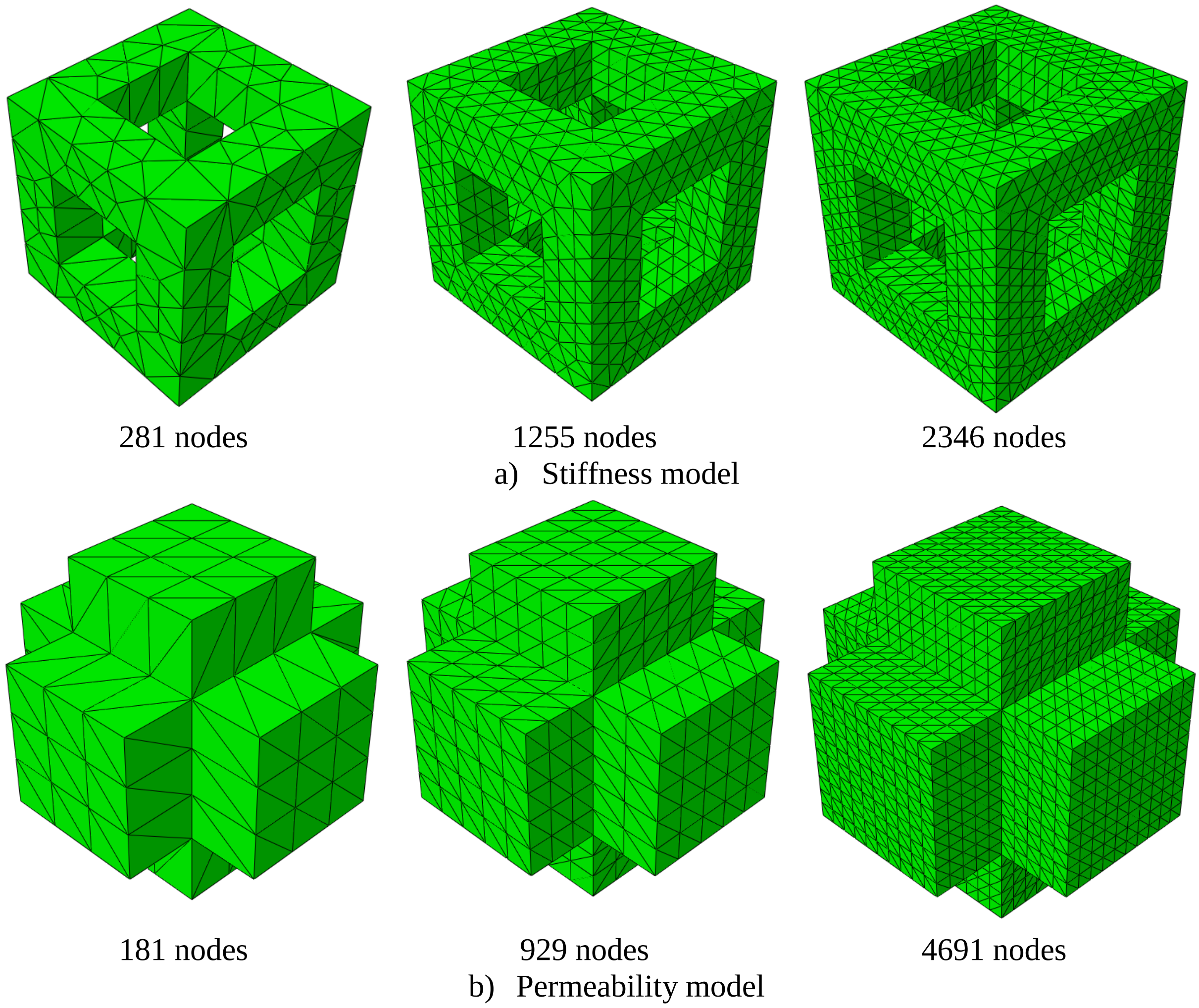

Figure 21: Domain discretization using tetrahedral element

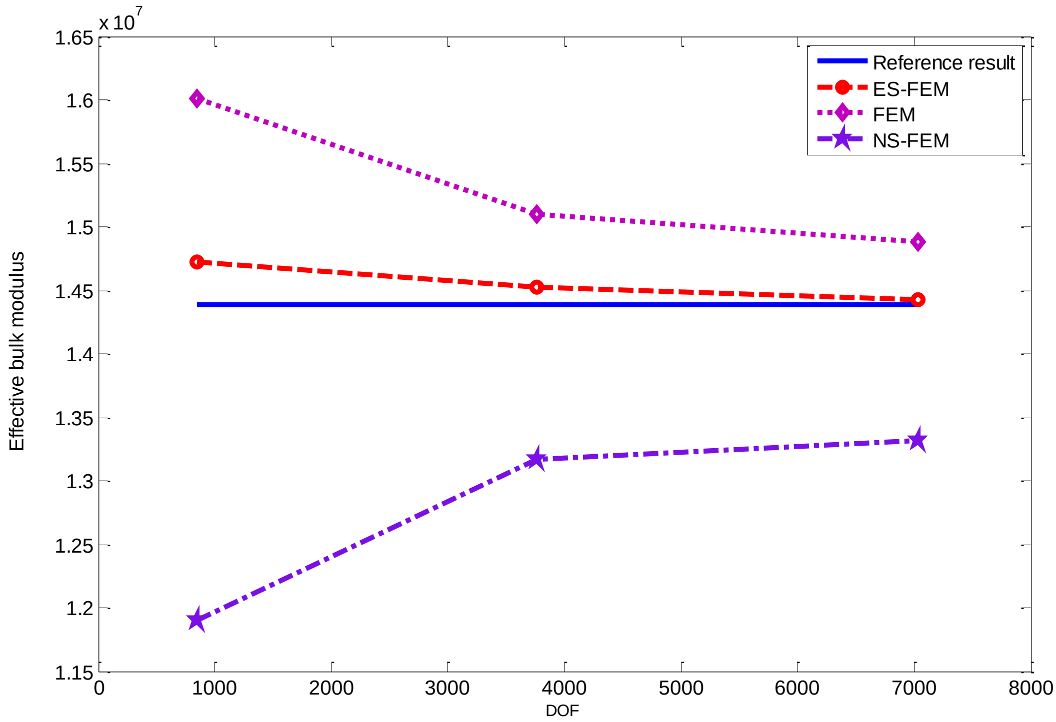

Figure 22: Convergence of effective bulk modulus

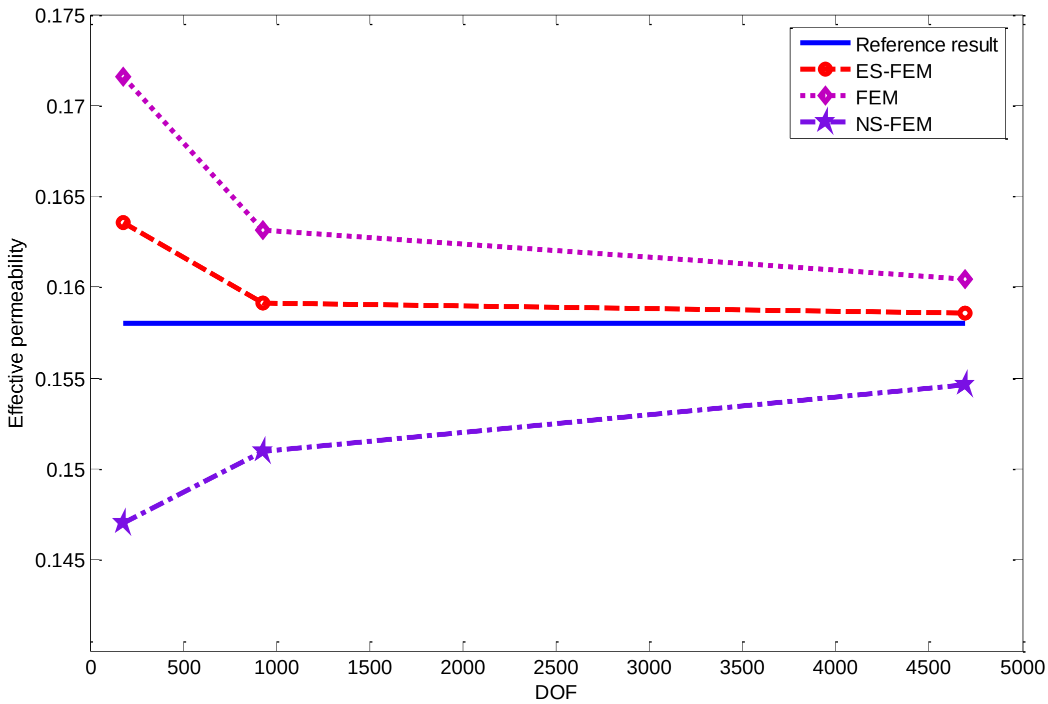

Figure 23: Convergence of effective permeability

Table

Table 1:Symmetry conditionsforthedifferentteststrains in 2D elasticity

Test strains	$x = 0,1$	$y = 0,1$
ε_{12}	$u_y^e = 0$	$u_x^e = 0$
$\varepsilon_{ij}, i = j$	$u_x^e = 0$	$u_y^e = 0$

Table 2:Symmetry conditionsforthedifferentteststrains in 3D elasticity [1]

Test strains	$x = 0,1$	$y = 0,1$	$z = 0,1$
ε_{12}	$u_y^e = u_z^e = 0$	$u_x^e = u_z^e = 0$	$u_z^e = 0$
ε_{23}	$u_x^e = 0$	$u_x^e = u_z^e = 0$	$u_x^e = u_y^e = 0$
ε_{13}	$u_y^e = u_z^e = 0$	$u_y^e = 0$	$u_x^e = u_y^e = 0$
$\varepsilon_{ij}, i = j$	$u_x^e = 0$	$u_y^e = 0$	$u_z^e = 0$

Table 3: Numerical results using different methods (Triangular element)

mesh	D_{11}^H	D_{12}^H	D_{22}^H	D_{33}^H	Methods
400 nodes T3	12.9527	3.2141	17.5111	2.7214	ES-FEM
400 nodes T3	13.1122	3.2948	17.6227	2.8669	FEM
400 nodes T3	12.4404	2.9412	17.1006	2.3718	NS-FEM
1387 nodes T3	12.8557	3.1472	17.4342	2.6556	ES-FEM
1387 nodes T3	12.9305	3.1926	17.4895	2.7142	FEM
1387 nodes T3	12.6398	3.0153	17.2643	2.5082	NS-FEM
8321 nodes T3	12.8181	3.1209	17.4057	2.6318	ES-FEM
8321 nodes T3	12.8447	3.1402	17.4269	2.6523	FEM
8321 nodes T3	12.7399	3.0640	17.3446	2.5765	NS-FEM

Table 4: Numerical results using different methods (Quadrilateral element)

mesh	D_{11}^H	D_{12}^H	D_{22}^H	D_{33}^H	Remarks
406 nodes T4	13.0335	3.2257	17.5535	2.7713	CS-FEM
406 nodes T4	13.1122	3.2948	17.6227	2.8032	FEM
406 nodes T4	12.5140	2.9605	17.1780	2.3793	NS-FEM
2341 nodes T4	12.8833	3.1375	17.4446	2.6901	CS-FEM
2341 nodes T4	12.9109	3.1388	17.4621	2.7129	FEM
2341 nodes T4	12.6777	3.0256	17.2966	2.5293	NS-FEM
9517 nodes T4	12.8599	3.1123	17.4168	2.6715	CS-FEM
9517 nodes T4	12.8876	3.1095	17.4310	2.6934	FEM
9517 nodes T4	12.7400	3.0631	17.3470	2.5768	NS-FEM

Table 5: Published results reported by other researches [9]

mesh	D_{11}^H	D_{12}^H	D_{22}^H	D_{33}^H	Remarks
20x20 4-node	13.015	3.241	17.552	2.785	Ref. [17]
1st adapt	12.910	3.178	17.473	2.714	Ref. [17]
2nd adapt	12.865	3.146	17.437	2.683	Ref. [17]
3rd adapt	12.844	3.131	17.421	2.668	Ref. [17]
436 8-node	12.839	3.139	17.422	2.648	HOMOG case (a)
305 8-node	12.820	3.124	17.407	2.634	HOMOG case (a)